Journal of Sustainable Development of Energy, Water and Environment Systems

http://www.sdewes.org/jsdewes

Year 2024, Volume 12, Issue 4, 1120516

Original Research Article

Enhancing Ciprofloxacin Removal: Unveiling the Potential of Graphene Oxide Synthesised from Cassava Peels through Box-Behnken Design Optimisation

Rinawati[1]*, Buhani[1], Widiarti[1], Ahmad Isro[1], Elsa Fitrianingsih[1], Anisa Rahmawati[1], Agung Abadi Kiswandono[1]*, Fidelis Nitti[2]*

[1]Department of Chemistry, Universitas Lampung, Bandar Lampung 35145, Indonesia
e-mails: rinawati@fmipa.unila.ac.id, buhani@fmipa.unila.ac.id, widiarti08@gmail.com, ahmadisro2409@gmail.com, fitrianingsih.elsa12@gmail.com, anisa.rw29@gmail.com, agung.abadi@fmipa.unila.ac.id

[2]Department of Chemistry, University of Nusa Cendana, Jl. Adi Sucipto, Penfui, Kupang 85001, Nusa Tenggara Timur, Indonesia
e-mail: fnitti@staf.undana.ac.id

Cite as: Rinawati, R., Buhani, B., Widiarti, W., Isro, A., Fitrianingsih, E., Rahmawati, A., Kiswandono, A. A., Nitti, F., Enhancing Ciprofloxacin Removal: Unveiling the Potential of Graphene Oxide Synthesised from Cassava Peels through Box-Behnken Design Optimisation, J.sustain. dev. energy water environ. syst., 12(4), 1120516, 2024, DOI: https://doi.org/10.13044/j.sdewes.d12.0516

ABSTRACT

The adsorption of ciprofloxacin from an aqueous solution using graphene oxide as an adsorbent derived from cassava peel waste using a modified Hummers method was described. The properties of the adsorbent were characterised using Fourier-Transform Infrared Spectroscopy, X-ray diffraction, Raman Spectroscopy and Scanning Electron Microscopy-Energy Dispersive X-ray techniques. The influence of the operational variables, including the potential of hydrogen, adsorbent mass, and contact time in the adsorption of ciprofloxacin, was evaluated by response surface methodology. In particular, the interactions between the operational variables were evaluated using the Box-Behnken Design to determine the optimum conditions. The results indicated that the optimum conditions were achieved at pH 3, with a contact time of 20 min, using 35 mg of graphene oxide adsorbent, resulting in an adsorption efficiency of 91.71%. The results demonstrated that the graphene oxide material derived from cassava peel waste can be effectively used as an adsorbent for ciprofloxacin from aqueous solutions.

KEYWORDS

Ciprofloxacin, Adsorption, Graphene oxide, Cassava peel waste, Box-Behnken Design.

INTRODUCTION

The contamination of water sources by pharmaceutical residues, particularly antibiotics, has become a growing concern due to its potential adverse effects on ecosystems and human health [1]. Antibiotic residues are introduced into the environment through diverse pathways, including the discharge of waste materials from healthcare facilities [2], pharmaceutical manufacturing processes [3], agricultural practices such as livestock farming, as well as the direct excretion of antibiotics by both human and animal populations [4]. The continuous utilisation of antibiotics in both human medical care and veterinary medicine has been linked to the growing demand for antibiotics and the consequent increase in antibiotic production, which in turn raises the likelihood of increasing levels of antibiotic residues in the environment. It is worth emphasizing that an estimated 75% to 95% of administered antibiotics undergo

incomplete metabolic breakdown or remain unmetabolised within the organisms [5]. This incomplete breakdown and the persistence of antibiotics within organisms contribute significantly to the release of antibiotic residues into the environment, thereby intensifying the problem of antibiotic contamination across various ecosystems. Thus, it is imperative to address the issue of antibiotic residues in aquatic ecosystems to ensure the continued availability of uncontaminated water, which is fundamental for sustaining all forms of life on Earth.

Among these antibiotics, ciprofloxacin (CIP) has garnered attention as a widely used fluoroquinolone-class antibiotic, known for its efficacy against a range of Gram-negative bacterial infections such as *Escherichia coli* and *Salmonella* spp, which are linked with a range of diseases, including gastroenteritis, urinary tract infections, and abdominal infections [6]. Additionally, CIP demonstrates notable efficacy against specific Gram-positive bacteria, particularly *Staphylococcus aureus* [7]. Notably, CIP exhibits high stability and water solubility across a wide range of pH conditions [8], leading to the anticipated presence of CIP residues in surface waters across diverse regions of Asia, Europe, and the Americas is a predictable occurrence. Typically, the global average concentration of CIP in freshwater surfaces falls within the range of 10−100 ng L^{-1}, with the highest recorded concentrations in lakes reaching levels between 2.5−6.5 mg L^{-1} [9]. The persistence of such antibiotic residues in the environment poses substantial risks, including the development of bacterial resistance, ecotoxicological implications, chondrogenic effects on wildlife, and the emergence of various diseases, such as intestinal and cutaneous infections in humans [10]. Therefore, despite the manifold advantages associated with CIP, it becomes imperative to develop methodologies for the removal of antibiotic residues, particularly from aquatic ecosystems, to safeguard human health and preserve existing ecological systems [11].

Numerous technologies have been proposed to address the removal of antibiotics. These include membrane-based approaches, such as the use of hybrid membranes composed of activated carbon and magnetic activated carbon for the removal of azithromycin [12], and the combination of membrane processes with advanced oxidation processes, adsorption, and biological treatments for the removal of active pharmaceutical ingredients [13]. In addition, electrochemical methodologies have also been employed for the removal of fluoroquinolone, ampicillin and chloramphenicol, as well as tetracycline [14]. This technique usually employs electrical energy to drive chemical reactions that degrade, transform, or remove antibiotic contaminants [15]. It relies on the use of electrodes to facilitate oxidation-reduction reactions and generate reactive species and has been proven highly effective in eliminating numerous persistent antibiotic pollutants [16].

Several advanced treatments, such as cavitation-based technologies, advanced oxidation processes, constructed wetlands, microalgae treatment, and microbial electrochemical systems, have also been explored for the removal of numerous antibiotics [17]. Cavitation-based technologies, relying on the use of bubble collapse in a liquid to create intense conditions that degrade contaminants, have been successfully employed to remove sulphadiazine, enrofloxacin and amoxicillin [18]. The mentioned techniques have also been thoroughly summarised for their application in the removal of tetracycline, involving the biodegradable and non-biodegradable routes [19]. Finally, adsorption techniques based on the use of numerous carbon-based absorptive materials like biochar, carbon nanotubes, activated carbon, and graphene have been proven effective in removing contaminants. However, challenges in process integration, production, and modification necessitate further research [20]. Adsorption-based methods, in particular, exhibit significant efficacy as they can eliminate both soluble, such as 4-nonylphenol [21] and insoluble biological contaminants and pollutants, such as estriol [22]. Moreover, adsorption processes offer the advantage of being straightforward to implement and cost-effective. Nevertheless, there remains a pressing need to develop methodologies that combine the use of low-cost natural adsorbents with high efficiency to tackle the removal of these pollutants.

Recent studies have highlighted the successful use of mesoporous or nanomaterials, such as Graphene Oxide (GO), in the removal of antibiotic pollutants [23]. In particular, numerous studies have explored the effectiveness of GO in adsorbing various antibiotics. Lebron *et al.* utilised statistical physics modelling to optimise the condition for the adsorption of norfloxacin onto GO. They found that norfloxacin adsorption occurs by a multi-molecule process with a 99% removal [24]. Gupta *et al.* optimised the removal of methadone using magnetic GO using response surface methodology and revealed that the optimum removal efficiency of methadone was 87.30 mg g^{-1} [25]. Salihi *et al.* employed GO for the adsorption of trimethoprim and isoniazid and obtained that the adsorption capacities for both compounds were 204.08 mg g^{-1} and 13.89 mg g^{-1}, respectively [26]. GO is a chemical compound known for its relatively polar and hydrophilic properties, primarily due to its abundant oxygen-containing groups, such as hydroxyl, epoxy, and carboxyl groups [27]. Typically, commercial production of GO involves the synthesis of pure graphite. However, achieving high-purity GO from natural-based sources can be challenging. Therefore, there is a need for alternative sources that are cost-effective and readily available and align with environmental considerations.

Agricultural waste represents one such environmentally friendly resource that can be harnessed as a raw material for producing GO. Adsorbents derived from agricultural waste not only contribute to the removal of antibiotic pollutants but also help in minimizing agricultural waste. Several studies have stated that agricultural waste that can be utilised as a source of adsorbents are wheat bran, banana peel, avocado peel, peanut shell, and sugarcane bagasse to remove lead (II) and chromium (VI) ions [28], cotton residues to remove methylene blue [29], and marigold flowers waste to remove cadmium (II) and chromium (VI) ions [30]. Cassava peel waste, for example, contains substantial carbohydrates, cyanide acid, protein, minerals, and sulphur groups, making it a suitable candidate for GO production [31]. Based on data from the Indonesian Central Statistics Agency in 2018, Lampung Province is one of the largest cassava producers in the country, with an impressive cassava production volume of approximately 6.68 million tons and an average yield of 25 tons per hectare each harvest season. This abundance underscores the potential of cassava peel waste as a valuable raw material for generating GO, which can serve as an efficient adsorbent for antibiotic pollutants, aligning with the region's high cassava production figures and the associated increase in cassava peel waste production. This research focuses on the use of cassava peel waste as a source for producing highly efficient GO-based adsorbent aimed at tackling antibiotic residues in aquatic environments. Specifically, this research centres on examining the adsorption of CIP on GO-based adsorbents synthesised via the modified Hummers method, while also exploring the influence of different operational conditions.

It is generally known that the adsorptive properties of any adsorbents are highly dependent upon active surface sites, including functional groups, particle size, and specific surface area [32]. The rich functional groups present in the active surface sites are important in the adsorption process as they facilitate specific interactions between the adsorbent and the target contaminants [33]. Moreover, the particle size and specific surface area of the adsorbent material significantly influence its adsorption capacity and efficiency, emphasizing the importance of designing the adsorbent material with suitable characteristics [34]. In the present research, the GO material derived from cassava peel waste was analysed using advanced analytical techniques, including Fourier Transform Infrared (FTIR) spectroscopy, Scanning Electron Microscopy-Energy Dispersive X-Ray (SEM-EDX), and X-ray Diffraction (XRD), to determine its properties and characteristics. Moreover, it is known that the optimum adsorption is highly dependent on process conditions such as pH, adsorbent mass, and contact time [35]. The impact of these operational variables on CIP adsorption using GO material was evaluated using response surface methodology (RSM), which establishes mathematical models correlating variables with responses to determine optimal process conditions [36]. In particular, the interactions between the operational variables were evaluated using the Box-Behnken Design (BBD) to determine the optimum conditions for CIP adsorption on GO. This approach

has been proven successful in optimizing diverse adsorption processes, including the removal of methadone from environmental samples [25], the treatment of textile waste contaminated with methylene blue [37], and the sequestration of heavy metals from aquatic environments [38].

MATERIALS AND METHODS

All chemicals used in this research were of analytical grade and were used as received without any further purification. The standard CIP was obtained from Hexpharm Jaya and was used to prepare the CIP standard solution. Other chemicals, such as iron (III) chloride hexahydrate ($FeCl_3 \cdot 6H_2O$), concentrated sulphuric acid (H_2SO_4), 30% hydrogen peroxide (H_2O_2), ethanol (C_2H_5OH), methanol (CH_3OH), were obtained from Supelco Sigma Aldrich and were used as received. Some other chemicals used in this research were potassium permanganate ($KMnO_4$), barium chloride ($BaCl_2$), and sodium hydroxide (NaOH) from MerckTM; 37% hydrochloric acid (HCl) and glacial acetic acid from Smart-Lab, and distilled water. The adsorbent materials used in this study were cassava peel waste obtained from local farmers in Lampung Province.

In this study, various equipment were employed, including an analytical balance (AND HR-150A with 152 g capacity and 0.1 mg precision), a hot plate magnetic stirrer (Stuart Biocote R200000 685), a centrifuge (Fisher Scientific 1827001027164), an oven (Memmert 55), a pH meter (Water Tester EZ-9901), and an ultrasonic device (1510 Branson). Several advanced analytical instruments such as Fourier Transform Infrared Spectroscopy (FTIR) instrument (Agilent Cary 630), Scanning Electron Microscope with Energy Dispersive X-ray (SEM-EDX) capability (EVO® MA 10), X-ray Diffraction (XRD) apparatus (XPERT PRO PANalytical PW3040/60), were employed in the characterisation of the resulting GO material. A UV-Vis Spectrophotometer (Agilent Cary 100) was used to determine CIP concentration in various samples.

The preparation of graphite from cassava peel waste

Cassava peel waste was washed thoroughly with water to remove impurities. Subsequently, the clean cassava peel waste was cut into small pieces and was left to air-dry under the sunlight for a period of 2 to 3 days. Following the initial drying phase, the cassava peels were further dried in an oven at 100 °C for 1.5 hours. Once completely dried, the cassava peels were crushed into smaller particles and then placed into a crucible cup with a total mass of approximately 6 g. The crushed material was subjected to high-temperature treatment, with the temperature reaching a maximum of 350 °C and maintained at this temperature level for 2 h. The resulting charcoal was allowed to cool for 15 min within a desiccator, and subsequently, it was finely ground using a mortar and sifted through a 100-mesh sieve.

A total of 5 g of the resulting carbon material obtained from the previous step was weighed and placed into a 1000 mL glass beaker. Subsequently, 500 mL of distilled water was added to the beaker, and the mixture was stirred at 600 rpm using a magnetic stirrer. To this suspension, 4 mL of 1 M $FeCl_3 \cdot 6H_2O$ solution was introduced. The addition of 4 mL of $FeCl_3 \cdot 6H_2O$ leads to the colour change into solid black. Transition metals, like iron, possess the capability to break the intra- and intermolecular hydrogen bonds in the cellulose of cassava peels at low temperatures. This procedure produces simpler molecules and a significant amount of long-chain alkanes, allowing the process to operate at lower temperatures.

Additionally, the interaction between iron and amorphous carbon leads to the formation of graphite structures. Such catalytic prowess underscores the exceptional performance of iron in the catalytic pyrolysis of solid waste, leading to the production of structured carbon nanomaterials [39]. However, the specific effects of iron in this procedure have not been thoroughly elaborated, presenting a challenge for future research aimed at improving the graphitisation process.

The stirring speed was then increased to 900 rpm while maintaining the mixture at room temperature. The pH of the combined solution was gradually adjusted to approximately a pH of 2 by the slow addition of 1 M HCl. The pH was adjusted to the targeted value, with measurements taken both initially and before each subsequent measurement. However, for large-scale production, it is crucial to maintain the pH of the solution using a buffer solution. The stirring continued at 900 rpm for 5 h at a temperature of 60 °C. Following this, the solution was subjected to centrifugation at 5000 rpm (2795 g) to separate the supernatant from the graphite precipitate. The precipitate was rinsed using distilled water until it reached a neutral pH of 7 and was subsequently filtered using filter paper. The resulting precipitate was then dried in an oven, initially at 50 °C for 8 h and subsequently at 110 °C for 5 h. Finally, the dried material was allowed to cool in a desiccator for 15 min [40].

The preparation of graphene oxide using the modified Hummers method

The synthesis of GO was performed by mixing 1 g of graphite with 23 mL of concentrated H_2SO_4 in a 500 mL beaker. This mixture was continuously stirred at 500 rpm using a magnetic stirrer and maintained at a cold temperature in an ice bath for 30 min. Subsequently, 3 g of $KMnO_4$ was slowly added into the mixture while the temperature was maintained below 10 °C. The stirring was then continued for an additional 30 min at 35 °C. The temperature of the mixture was increased by a slow addition of 46 mL of distilled water until the temperature reached 98 °C, after which the mixture was maintained at room temperature for about 15 min [41].

To further enhance the optimisation of the oxidation reaction, 140 mL of distilled water was added to the mixture. While being stirred at 500 rpm with a magnetic stirrer for 10 min, 10 mL of a 30% H_2O_2 solution was slowly added. The resulting suspension was then washed multiple times using a 5% HCl solution to remove sulphate ions. This effect was confirmed by testing the suspension with $BaCl_2$ solution to ensure the absence of sulphate ions, which was indicated by the absence of a white precipitate. Subsequently, the material was thoroughly rinsed with distilled water until it reached a pH of 5. The solution was then subjected to centrifugation at 5000 rpm for 10 min to separate the precipitate. The resulting precipitate was dispersed in 450 mL of distilled water, subjected to sonication for 30 min, and then filtered using filter paper. The separated precipitate was subsequently dried in an oven at 60 °C for 5 h [42].

The characterisation of graphene oxide

The resulting GO material was further analyzed using several advanced analytical instruments to determine its properties and characteristics. The analysis of functional groups of the GO material was performed using the FTIR instrument. The morphological characteristics, elemental content, and quantitative composition of the GO were assessed using SEM-EDX. It enables a comprehensive examination of the material's surface and its elemental components. An XRD technique was employed to examine the material's structural arrangement and crystalline properties of the GO material to assess the extent of its crystallinity.

Box-Behnken Design

The experimental design employed the Box-Behnken Design (BBD) method, which involves varying variables at three levels: high (+1), medium (0), and low (−1), with five additional central repetition points, as outlined in **Table 1**. The design generated a total of 17 experiments based on the specified values derived from the BBD procedure. These experiments were carefully and precisely planned using the Design-Expert software (DX7).

Table 1. Selected levels of independent variables in BBD

Influencing factors	-1	0	1
Adsorbent dose [mg]	20	27.5	35
pH [-]	2	3	4
Contact time [min]	20	30	40

The experiments were performed sequentially, following the prescribed values outlined in **Table 1** of the BBD design. For each sample, a specific concentration of the antibiotic CIP solution was mixed with a designated quantity of the GO adsorbent under controlled pH conditions and for a specified contact time. The solutions with pH values of 2, 3, and 4 were prepared by the addition of dropwise of HCl until reaching the desired solution's pH. Subsequently, the GO was separated through a combination of centrifugation and filtration methods, allowing for the measurement of the remaining antibiotic concentration in the solution using a UV-Vis spectrophotometer set at a wavelength of 277 nm. A fit analysis was conducted to assess the accuracy and validity of the obtained results, establishing the percentage of antibiotic adsorption as the response variable, see eq. (1).

$$Adsorption\ \% = \frac{C_0 - C_x}{C_0} \times 100 \tag{1}$$

Where C_0 and C_x represent the initial and final concentrations of CIP in solution [ppm].

RESULTS AND DISCUSSION

In this section, the results of the research were provided, and a comprehensive analysis of the results was conducted to reveal significant insights into the underlying trends and implications of the findings. These include the characteristics of the synthesised GO material based on the measurements' results using several analytical instruments, including FTIR, SEM, and XRD. After that, a detailed discussion was conducted on the optimisation of the adsorption condition of CIP using GO, with a comprehensive comparison with the experimental data.

Graphene oxide characterisation

The obtained GO was then further characterised using FTIR, SEM, and XRD instruments and the results are shown in **Figure 1**. **Figure 1a** shows the FTIR characterisation results of commercial graphite, biomass graphite and GO. Both FTIR of graphite biomass and GO spectra exhibit absorption characteristics of the stretching vibration of the −OH (hydroxyl) group, as evident by the peaks at 3198 cm^{-1} and 3205 cm^{-1}. The presence of the −OH group in GO spectra can be attributed to the presence of water (H_2O) within the GO structure **[41]**. Furthermore, there is absorption at 1699 cm^{-1}, indicating the absorption of C=O (carbonyl) groups in GO spectra. The observed absorptions at 1595 cm^{-1} and 1028 cm^{-1} in GO's spectra demonstrate the presence of C=C (alkene) and C−O−C (epoxy) groups in the generated GO. As was previously mentioned, the functional groups in the GO from the modified Hummers method have oxygen groups, namely carbonyl (−C=O), carboxyl (−COOH), and hydroxyl (−OH). This FTIR spectrum shows that the manufacture of GO was successful since it has a functional group that is suitable for pure GO **[43]**. In accordance with the results reported by Sujiono *et al.* **[41]** and Surekha *et al.* **[44]**, it is established that GO contains oxygen-based functional groups, encompassing carbonyl (−C=O), carboxyl (−COOH), hydroxyl (−OH), and epoxy (C−O−C) groups. The similarity observed in the FTIR spectra of graphite and the produced GO can be attributed to several factors, including minor impurities, surface functional groups, or structural defects present in graphite samples, which can result in weak peaks or absorption bands in the FTIR spectrum. These features, though often subtle, may be observable and have been evident in graphite from biomass, studied by Kanta *et al.* **[45]**, Kim *et al.* **[46]**,

and Hedge *et al*. [47]. This situation starkly contrasts with commercial graphite, sourced independently of biomass, which lacks peaks associated with functional groups (Figure 1). The differentiation between the spectra of graphite and GO becomes apparent with the appearance of epoxy peaks absent in the graphite spectrum. While not distinctly visible in the FTIR spectrum, the augmentation of functional groups in the resultant GO is discernible through the outcomes of EDX analysis.

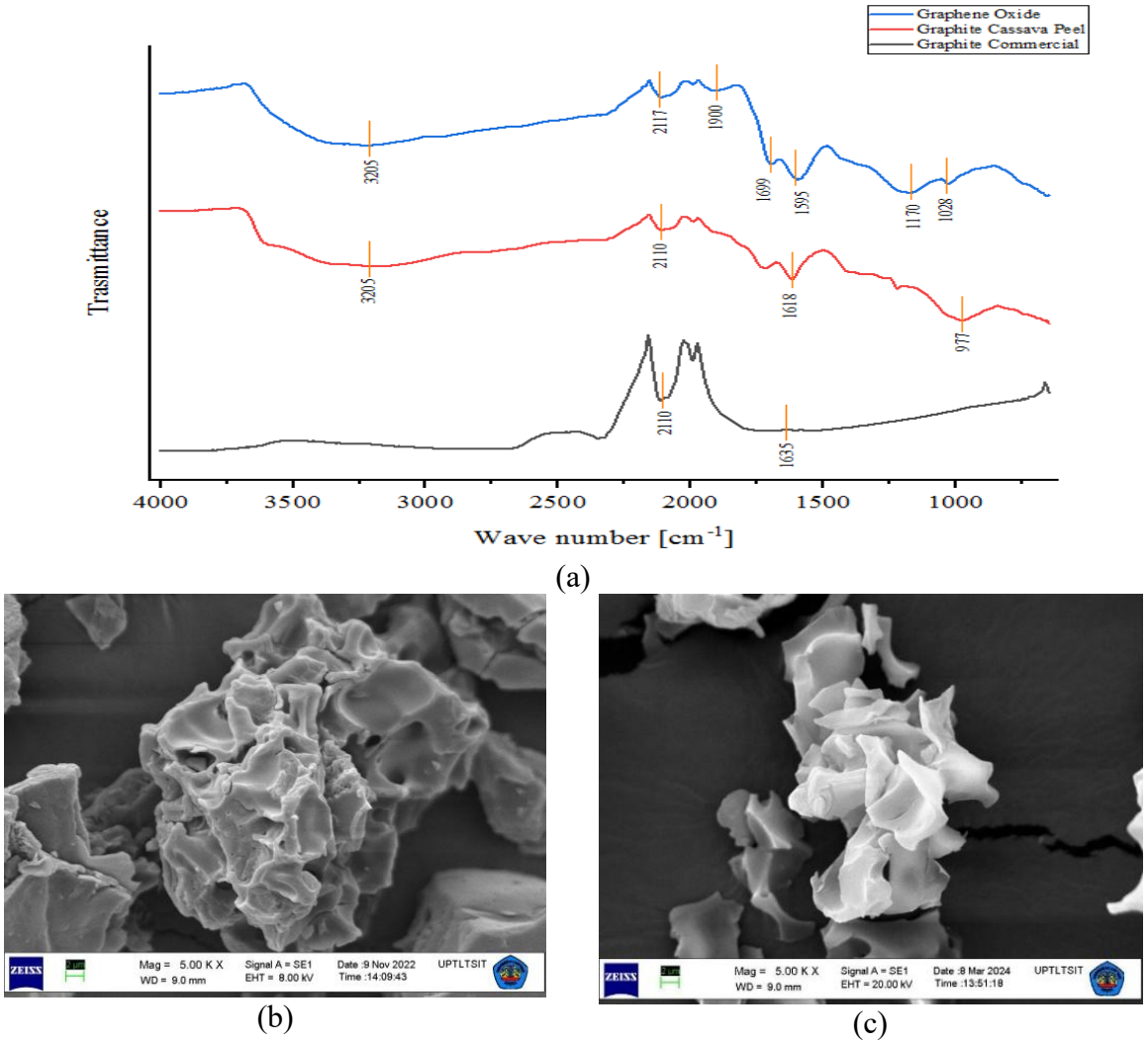

Figure 1. FTIR spectra of graphite and GO (a), SEM image of graphite (b), SEM image of GO (c); GO made from cassava peel waste using modified Hummers method

The surface morphology of graphite and GO is visualised in Figures 1b and 1c. The graphite surface morphology (Figure 1b) appears to resemble chunks with flakes that have sharp edges and there are wrinkled areas. The surface morphology of GO at 5000× magnification (Figure 1c) exhibits a stack of thin sheets with a smooth surface and areas with slight wavy wrinkles. This image also shows that samples exhibit strata with different levels of transparency, as previously reported in [48]. In addition, the surface of GO has many curved shapes and protrusions. The formation of a sheet pile indicates that peeling has occurred during the oxidation and sonication process.

The EDX spectra and elemental weight percentages were obtained for graphite and GO derived from cassava peels, as illustrated in Figure 2. The EDX analysis of graphite only revealed the presence of carbon and oxygen atoms (Figure 2a). In contrast, GO exhibited the

presence of carbon and oxygen atoms alongside potassium and manganese atoms (**Figure 2b**). The latter may have originated from the reagents employed in the oxidation process. Upon subjecting graphite to oxidation via the Hummers method, the weight percentage of carbon decreased to 77.62%, while that of oxygen increased to 22.32%. This elevation in oxygen content suggests the occurrence of the oxidation process in graphite, resulting in the formation of GO.

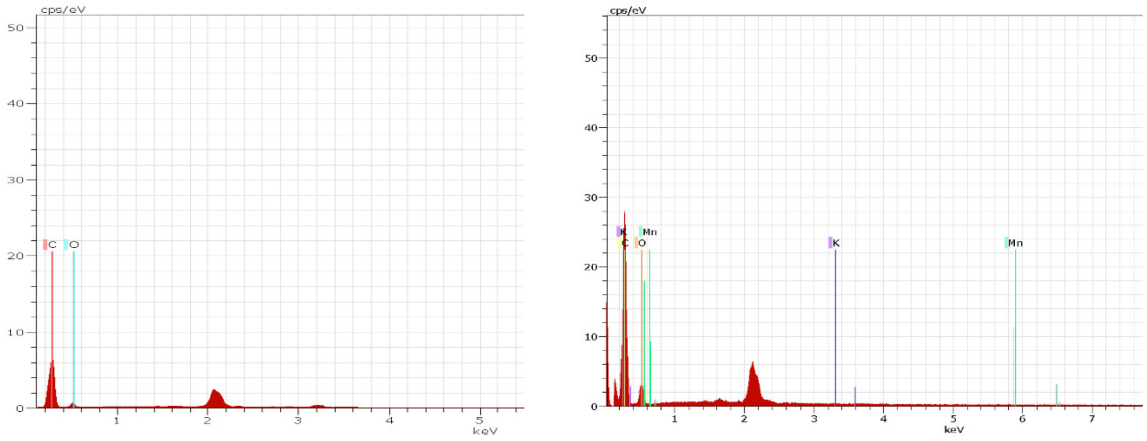

(a) (b)

Figure 2. The EDX spectra of graphite (a) and GO (b)

The X-ray diffraction (XRD) spectrum of GO is depicted in **Figure 3a**. The XRD is a powerful method generally employed to examine the crystalline structure of a certain material. The XRD diffraction patterns can reveal an amorphous structure evidenced by broad peaks observed at 2θ values [49]. Here, the XRD diffractogram pattern exhibits carbon peaks at 2θ values of 24.20° and 38.91°, which are characteristic peaks for carbon materials [50]. This pattern coincides with the results reported by Özgan and Eskalen [51], where the XRD pattern of GO exhibited a crystalline peak at 2θ of 12.78°. A comparison with the research conducted by Sujiono *et al.*, which involved the synthesis of GO from waste coconut shell graphite, reveals a similar amorphous peak at 2θ of 23.97° [41]. The differences in 2θ values are attributed to the utilisation of graphite derived from natural resources (agricultural waste) rather than commercial graphite [52].

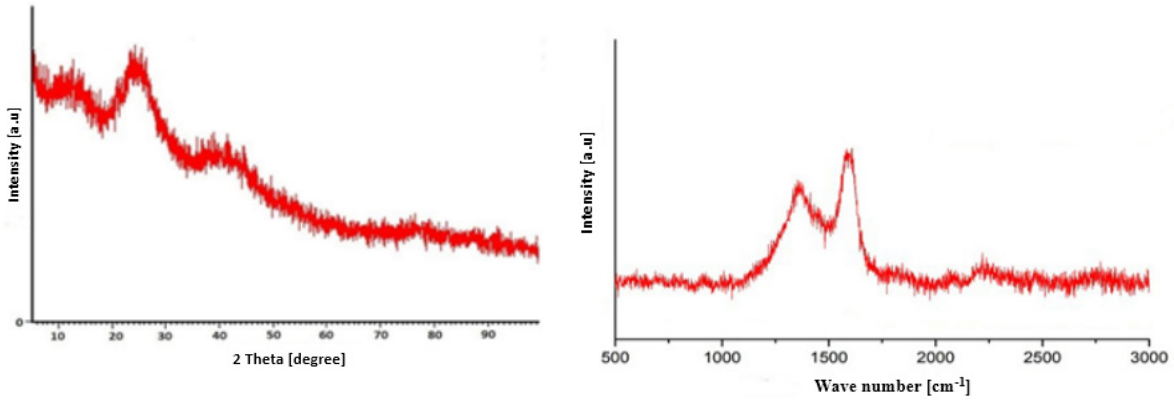

(a) (b)

Figure 3. The XRD spectrum (a) and Raman spectrum (b) of GO made from cassava peel waste using modified Hummers method

The Raman spectrum of GO is seen in **Figure 3b**. Two peaks, representing the D band and the G band, can be seen in the picture at wave numbers 1363 cm^{-1} and 1598 cm^{-1}, respectively. In graphite, vibrational modes associated with edges, concomitant impurities, and structural defects give rise to the D band. The characteristic D-bands of graphene sheets indicate that the sp^3 carbons have been stretched. The graphic makes the G-bands, which are caused by vibrations in the normal graphite structure, more evident. It is like trying to stretch sp^2 carbon. These two peaks indicate the presence of sp^2-hybridised carbon in the reported GO, which is consistent with conventional Raman vibrational modes for carbon-based materials. The Raman results of this study are in line with the approach used by Sujiono *et al.* **[41]** to characterise GO derived from leftover coconut shells and with the application of GO derived from sugarcane bagasse by Somanathan *et al.* **[53]**.

Experimental design and optimisation using Box-Behnken Design

In this subsection, the outcomes of the experimental design and the effects of process variables and their interactions on CIP adsorption are discussed.

Analysis of the responses (ANOVA). The results of the optimisation of CIP adsorption, conducted through the BBD experimental approach involving 15 experiments, can be found in **Table 2**. The relationship between the response or CIP antibiotic adsorption and the three operational variables, namely adsorbent dose, pH, and contact time, was evaluated using Response Surface Methodology (RSM). The use of RSM, specifically based on the BBD experimental design, aims to showcase the optimisation process conditions for CIP antibiotic adsorption.

Table 2. The results of the Box-Behnken experimental design

Run	Adsorbent dose [mg]	pH	Contact time [min]	Adsorption [%]
1	27.5	4	40	85.10
2	20	4	30	84.07
3	35	2	30	75.12
4	20	2	30	60.02
5	20	3	40	83.40
6	35	3	20	91.71
7	27.5	3	30	80.25
8	27.5	4	20	88.28
9	35	4	30	83.41
10	27.5	3	30	84.97
11	27.5	2	20	78.51
12	20	3	20	86.92
13	27.5	3	30	77.13
14	27.5	2	40	76.90
15	35	3	40	90.24

The outcomes of the experimental design and the subsequent statistical analysis, employing a quadratic statistical model as derived from the software, are expressed in eq. (2). In this equation, a positive sign associated with a variable signifies a synergistic influence on the target, while a negative sign indicates that the variable exerts an antagonistic impact **[54]**.

$$\% \text{ CIP Adsorption} = 80.78 + 3.26A + 6.29B - 1.22C - 3.94AB + 0.03925BC + 0.3708A^2 - 5.50B^2 + 6.91C^2 \quad (2)$$

Where A denotes adsorbent dose [mg], B − pH, and C − contact time [min].

Table 3. Results of analysis of variance (ANOVA)

Source	Sum of Squares	df	Mean Square	F-value	p-value	
Model	788.90	9	87.66	7.56	0.0192	significant
A	84.96	1	84.96	7.33	0.0424	
B	316.39	1	316.39	27.29	0.0034	
C	11.96	1	11.96	1.03	0.3564	
AB	62.09	1	62.09	5.36	0.0685	
AC	1.05	1	1.05	0.0906	0.7755	
BC	0.6162	1	0.6162	0.0532	0.8268	
A^2	0.5078	1	0.5078	0.0438	0.8425	
B^2	111.66	1	111.66	9.63	0.0267	
C^2	176.47	1	176.47	15.22	0.0114	
Residual	57.96	5	11.59			
Lack of Fit	26.80	3	8.93	0.5735	0.6855	not significant
Pure Error	31.16	2	15.58			
Cor Total	846.86	14				

Std Dev = 3.40, R^2 = 0.9316, Adj R^2 = 0.8084, CV% = 4.17, Pred R^2 = 0.4108, Adeq Precision = 10.7441

It is evident from **Table 3** that the proposed model is statistically significant, with a total quadratic model sum of 788.90 and an F-value of 7.56. The p-value serves as a crucial indicator for evaluating the significance of each coefficient. The p-values less than 0.05 indicated a significant and well-fitting model **[55]**. In the present research, the operational variables such as adsorbent dose (A), pH (B), the square of pH (B^2), and the square of contact time (C^2) exhibit p-values below 0.05, underscoring their significance. Conversely, the remaining variables display p-values exceeding 0.1, suggesting their lack of significance. Consequently, model refinement can be undertaken by eliminating the non-significant variables to enhance the model's performance.

The results indicated that the R-squared (R^2) value was 0.9316, which signifies a good fit of the model with the experimental data. It is important to note that the difference between the predicted R^2 and the adjusted R^2 should be less than 0.2. The difference exceeding 0.2 indicated a potential issue with either the model or the experimental data. The Adeq Precision value obtained in this research was 10.7441 (greater than 4), suggesting a favourable agreement between experimental results and predictions. With a coefficient of variation (CV%) of 4.17% (less than 10%), there exists a notable correlation between the experimental response and model predictions. Moreover, the lack of fit, when compared to pure error, yields an insignificant F-value (0.6855). In order to establish a robust model, it is crucial for the lack of fit to be non-significant.

The results obtained from the diagnostic tests shown in **Figure 4** provide insight into the model's adequacy. These diagnostic assessments include (a) the normal probability plot of Student residuals, (b) residuals versus predicted, (c) residuals versus run number, and (d) measured values. These diagnostics collectively support the notion that the model performs well and support the ANOVA test results obtained in **Table 3**. The normal distribution graph shows favourable outcomes for the experiments conducted on % CIP Adsorption because the generated values align closely with the straight line. **Figures 4b** and 4c also indicate that the experiments exhibit a homogeneous distribution because the spread of values generated

approaches zero. The residual values show a normal distribution of the applied variables, approaching the mean value. Therefore, one of the proposed models for predicting CIP adsorption efficiency is a regression model [54]. The regression value obtained is 0.9316, as evident in **Figure 4d**. The R^2 value indicates the quality of fit in a model. The criteria for a good fit model are $R^2 > 0.8$, and R^2 approaching 1 indicates a high level of agreement between experimental data and the proposed model [56].

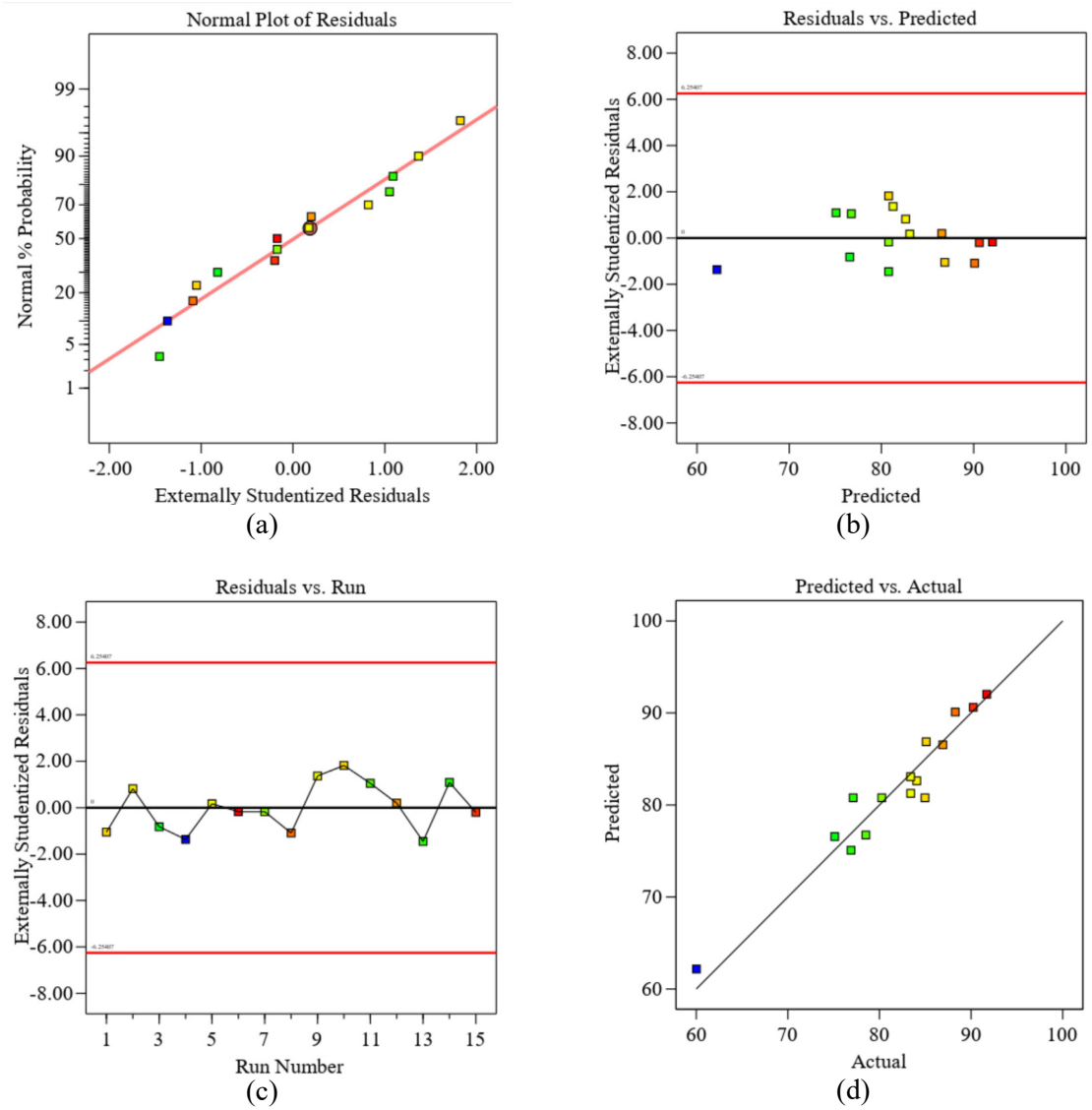

Figure 4. The results of diagnostic tests: normal probability of Student residuals (a), residuals versus predicted (b), residuals versus run number (c), measured values (d)

Interactions between process variables and their effect on CIP Removal. The three-dimensional reaction surface plots offer insights into the primary influences of three key factors. A series of experiments were conducted to assess the impact of adsorbent dosage on adsorption efficiency, using adsorbent quantities ranging from 20 to 35 mg at pH levels of 2.0, 3.0, and 4.0, with contact times set at 20, 30, and 40 min. The interactive effect of pH and dosage on CIP removal is illustrated in **Figures 5a** and **5b**. The results revealed that higher levels of adsorbent dose exceeding 29 mg and elevated pH levels beyond 2.5 are associated with increased CIP removal.

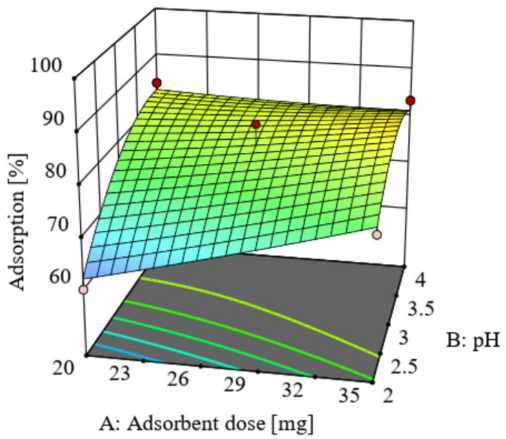

X1: A = Adsorbent dose [mg]
X2: B = pH
Actual Factor: C = 30 min

(a)

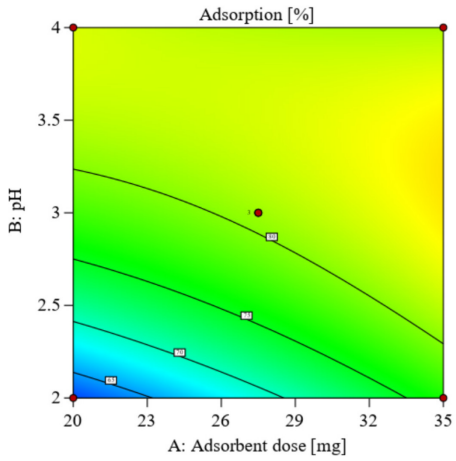

X1: A = Adsorbent dose [mg]
X2: B = pH
Actual Factor: C = 30 min

(b)

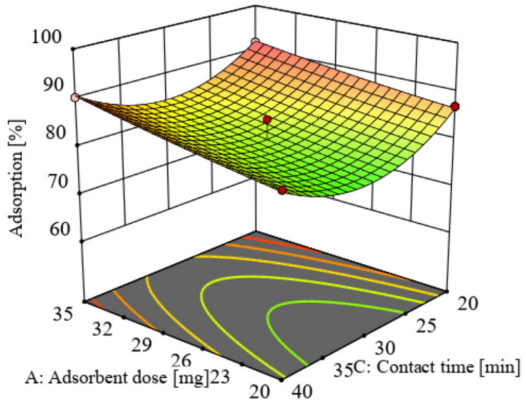

X1: A = Adsorbent dose [mg]
X2: C = Contact time [min]
Actual Factor: B = 3

(c)

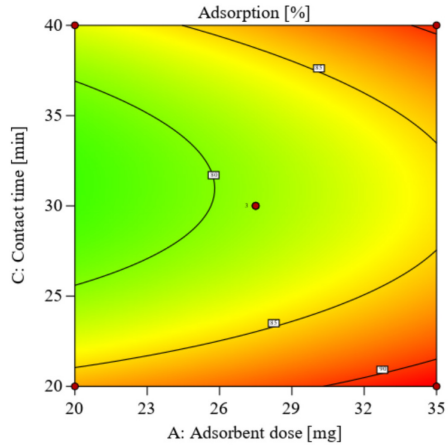

X1: A = Adsorbent dose [mg]
X2: C = Contact time [min]
Actual Factor: B = 3

(d)

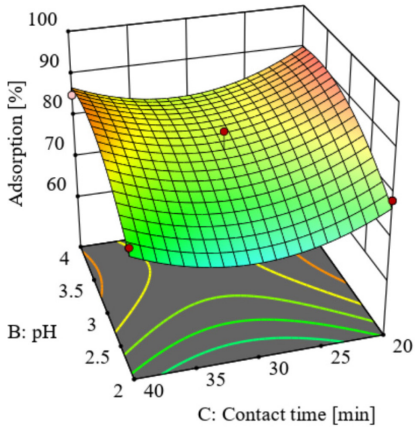

X1: B = pH
X2: C = Contact time [min]
Actual Factor: A = 27.5 mg

(e)

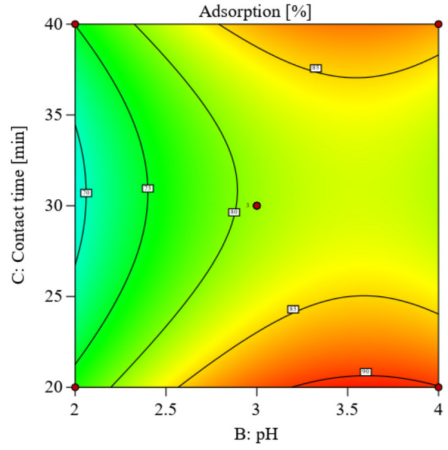

X1: B = pH
X2: C = Contact time [min]
Actual Factor: A = 27.5 mg

(f)

Figure 5. Response surface plots (3D) and contour plots (2D): interaction between adsorbent dose and pH (a, b), interaction between adsorbent dose and contact time (c, d), interaction between pH and contact time (e, f)

Konkena and Vasudevan (2012) reported a high correlation between the pH value and different functionalities on GO with pH values of 4.3, 6.6, and 9.8. Below a pH of 2, carboxyl groups remain undissociated, while above pH 4, they start to dissociate. This observation indicates that the surface of GO becomes negatively charged under acidic conditions, especially after the pH exceeds 4. The negatively charged surface of GO enhances interactions with positively charged CIP under acidic conditions. Therefore, even though the pH range in this study was selected as pH 2−4, it is necessary to test the adsorption capacity of GO over a wider pH range to maximise the potential for CIP adsorption onto GO. However, selecting pH conditions from acidic to neutral is more favourable as it corresponds to the positively charged nature of CIP and the negatively charged surface of GO. Under acidic conditions, GO is advantaged due to its stable dispersibility compared to other conditions [57].

Furthermore, the interactive effect of dosage and contact time on CIP removal is depicted in Figures 5c and 5d. At lower contact times (less than 2.5 min) or longer contact times (greater than 3.5 min), higher doses of the adsorbent are preferable to achieve higher CIP removal efficiency. Figure 5d also indicates the possibility of achieving optimal CIP removal at adsorbent doses exceeding 35 mg. The curvature of the surface plot in Figures 5e and 5f demonstrates the interactive effect of pH and contact time on CIP removal. The removal efficiency is notably low within the range of 25−35 min of contact time and at lower pH levels. In contrast, at shorter contact times (below 25 min) or extended contact times (beyond 35 min), higher pH levels, specifically above 2.5, are preferred to attain higher CIP removal efficiency.

Optimisation of the responses. The optimisation of responses was carried out using the desirability approach. In this approach, the total desirability is calculated as the geometric mean of all individual desirability values, with individual desirability scores ranging from 0 (indicating the least desirable) to 1 (representing the most desirable) [55]. The highest desirability is depicted in a graphical form, as shown in Figure 6. The results obtained align with the experimental data, indicating that the ideal conditions for CIP removal were achieved at a pH level of 3 and a contact time of 20 minutes, using 35 mg of adsorbent. Under these conditions, the maximum CIP concentration removed was determined to be 91.71%.

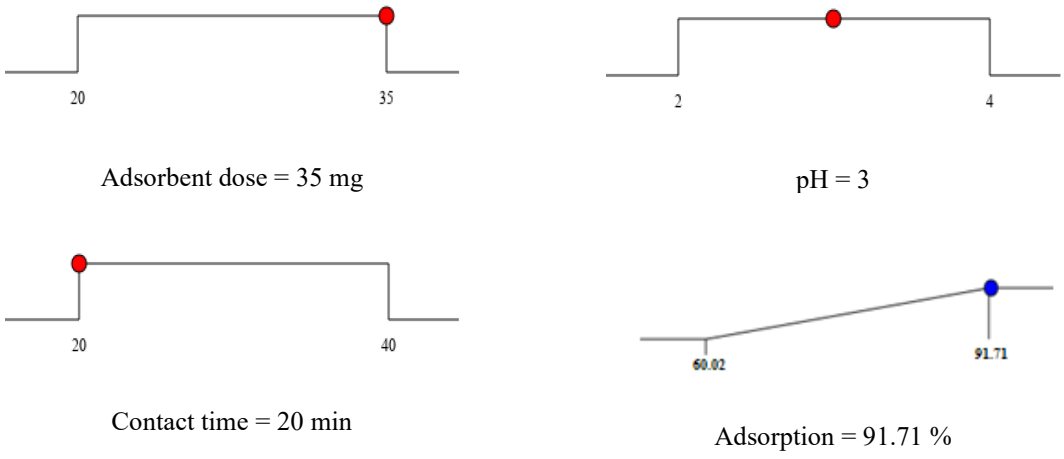

Figure 6. Ramp solution for desirability approach; desirability = 1.000

Effect of variables and their interactions. The amount of adsorbent used in the adsorption process varies depending on the specific adsorbate and is influenced by its physical and chemical characteristics. In the case of CIP (Ciprofloxacin) adsorption, the adsorbent dosage plays a significant role. When a dose of 35 mg of adsorbent was utilised at pH 3 with a contact time of 20 minutes, the percentage of CIP adsorption reached 91.71%. This enhanced adsorption can be attributed to the greater number of active sites and increased surface area

available on the adsorbent, facilitating more effective adsorption. Carbon-based materials are known to have outstanding adsorption characteristics, making them highly effective in eliminating antibiotics not only at low environmental concentrations but also at elevated concentrations. The presence of C=C functional groups in both carbon-based materials and antibiotics plays a crucial role in influencing the adsorption rate. An increased number of aromatic rings corresponds to a higher adsorption rate [58].

CIP exhibits a positive charge when the pH is below 5.90, transitions to a neutral or zwitterionic state between pH 5.90 and 8.89, and carries a negative charge at pH levels above 8.89, as depicted in Figure 7 [59]. The highest adsorption of CIP is observed around neutral and acidic pH levels. In particular, under acidic conditions, the amine group in CIP will be protonated (NH_3^+) and inhibit its ionic interaction with GO adsorbents containing carboxyl groups [60]. At pH 5, about 80% of the carboxyl groups are deprotonated (COO^-) and become negatively charged [43]. This phenomenon can be attributed to the ionic state and interactions occurring between the amine groups on CIP and the carboxylate groups on GO [60]. However, as the pH increases, the positive charge on CIP decreases, leading to a reduction in electrostatic interactions and consequently decreasing the adsorption capacity.

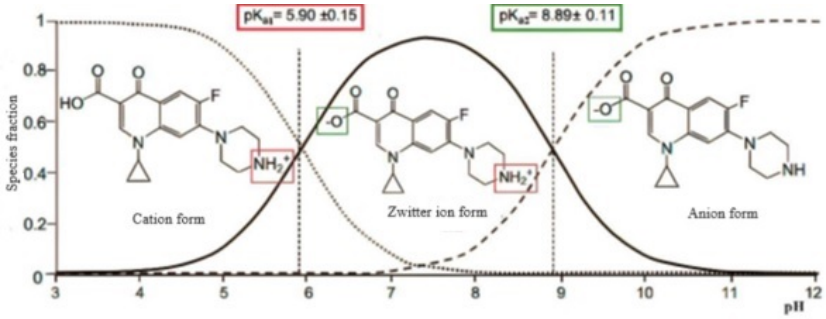

Figure 7. The variation of CIP into distinct forms or types at various pH levels [61]

The contact time also has a significant influence on CIP adsorption. When using an adsorbent dose of 35 mg and a pH of 3, a 40-minute contact time resulted in a CIP removal efficiency of 90.24%. However, when maintaining the same conditions but reducing the contact time to 20 minutes, the CIP removal efficiency increased to 91.71%, as evident in Table 2. This phenomenon can be attributed to the initial abundance of available active sites on GO during the early stages of CIP uptake. Subsequently, the adsorption rate slows down after 40 minutes, likely due to a reduction in available active sites over time, ultimately leading to adsorbent saturation [62].

CONCLUSIONS

The optimisation of CIP adsorption onto GO derived from cassava peel, employing a Box-Behnken Design (BBD) experimental approach, has yielded optimal conditions for CIP removal. These conditions include a pH level of 3, a contact time of 20 minutes, and the utilisation of 35 mg of adsorbent material. The GO derived from cassava peel is rich in functional groups like hydroxyl, carboxyl, and epoxy, which provide robust adsorption capabilities through their active sites. Under these optimised parameters, a remarkable CIP concentration removal efficiency of 91.71% was achieved, highlighting the potential of the GO material obtained from cassava peel to be effectively used as an adsorbent for CIP from aqueous solutions. However, it is important to note that further research is needed to test the performance of GO on larger scales and various environmental conditions to ensure its sustainability in practical applications.

The restrictive pH range for effective adsorption is one of the key requirements for efficient CIP removal treatment in wastewater. It may involve adjusting the pH of the influent

wastewater to maintain conditions favourable to GO adsorption. This approach could necessitate the addition of acids or bases to the influent stream to achieve the desired pH level.

The results of this research provide important implications in the context of environmental protection and public health. The use of CIP as an antibiotic can increase bacterial resistance and have a negative impact on aquatic organisms and human health if it accumulates in wastewater. Therefore, GO's effective ability to remove CIP can help reduce the risk of antibiotic contamination in the water cycle, as well as reduce its negative impact on the environment and public health.

Overall, this study highlights the significant potential of the GO material obtained from cassava peel to be effectively used as an adsorbent for CIP removal from aqueous solutions. By understanding the optimal conditions for CIP adsorption, we hope that these findings will provide a valuable contribution to the development of more effective and sustainable wastewater treatment methods in the future.

DECLARATION OF COMPETING INTEREST

The authors declare that they have no known competing financial interests or personal relationships that could have appeared to influence the work reported in this paper.

ACKNOWLEDGEMENT

The author would like to thank the Directorate for Research, Technology and Community Services, The Ministry of Education, Cultural, Research and Technology, Republic of Indonesia, for funding this research through the Penelitian Dasar Unggulan Perguruan Tinggi (PDUPT) research scheme with contract number of 0357/E5/AK.04/2022 and 2147/UN26.21/PN/2022. Assistance from various parties who directly or indirectly supported the completion of this research was also acknowledged.

NOMENCLATURE

Symbols

C_o	initial concentration of ciprofloxacin in solution	[ppm]
C_x	final concentration of ciprofloxacin in solution	[ppm]

Abbreviations

BBD	Box-Behnken Design
CIP	Ciprofloxacin
FTIR	Fourier Transform Infrared
GO	Graphene Oxide
RSM	Response Surface Methodology
SEM-EDX	Scanning Electron Microscopy-Energy Dispersive X-ray
UV-Vis	Ultraviolet-Visible
XRD	X-ray Diffraction

REFERENCES

1. Yeo, J. Y. J., Khaerudini, D. S., Soetaredjo, F. E., Waworuntu, G. L., Ismadji, S., Putranto, A., and Sunarso, J., Experimental and Modelling Study of Adsorption Isotherms of Amoxicillin, Ampicillin and Doripenem on Bentonite-Chitosan Composite. S. Afr. J. Chem. Eng., vol. 43, pp. 38-45, 2023, https://doi.org/10.1016/j.sajce.2022.09.013.
2. Wong, S. L., Mohamed Noor, M. H., Ngadi, N., Mohammed Inuwa, I., Mat, R., and Saidina Amin, N. A., Aspirin Adsorption onto Activated Carbon Derived from Spent Tea Leaves: Statistical Optimization and Regeneration Study. Int. J Environ. Res., vol. 15, pp. 413-426, 2021, https://doi.org/10.1007/s41742-021-00325-1.

3. Ebele, A. J., Oluseyi, T., Drage, D. S., Harrad, S., and Abdallah, M. A.-E., Occurrence, Seasonal Variation and Human Exposure to Pharmaceuticals and Personal Care Products in Surface Water, Groundwater and Drinking Water in Lagos State, Nigeria. Emerg. Contam., vol. 6, pp. 124-132, 2020, https://doi.org/10.1016/j.emcon.2020.02.004.
4. Foroush, M. P., Ahmadi, R., Yousefi, M., and Najafpour, J., In Silico Study of Adsorption of Penicillin Antibiotic on the Surface of Single Walled Nitride Boron Nanotubes(Sbnnt). S. Afr. J. Chem. Eng., vol. 37, pp. 135-140, 2021, https://doi.org/10.1016/j.sajce.2021.05.007.
5. Marshall, B. M. and Levy, S. B., Food Animals and Antimicrobials: Impacts on Human Health. Clin. Microbiol. Rev., vol. 24, no. 4, pp. 718-733, 2011, https://doi.org/10.1128/cmr.00002-11.
6. Kutuzova, A., Dontsova, T., and Kwapinski, W., Application of Tio2-Based Photocatalysts to Antibiotics Degradation: Cases of Sulfamethoxazole, Trimethoprim and Ciprofloxacin. Catalysts, vol. 11, no. 6, p. 728, 2021, https://doi.org/10.3390/catal11060728.
7. Johansson, C. H., Janmar, L., and Backhaus, T., Toxicity of Ciprofloxacin and Sulfamethoxazole to Marine Periphytic Algae and Bacteria. Aquat. Toxicol., vol. 156, pp. 248-258, 2014, https://doi.org/10.1016/j.aquatox.2014.08.015.
8. Zhuang, Y., Yu, F., Ma, J., and Chen, J., Adsorption of Ciprofloxacin onto Graphene–Soy Protein Biocomposites. New J. Chem., vol. 39, no. 5, pp. 3333-3336, 2015, https://doi.org/10.1039/C5NJ00019J.
9. Kovalakova, P., Cizmas, L., McDonald, T. J., Marsalek, B., Feng, M., and Sharma, V. K., Occurrence and Toxicity of Antibiotics in the Aquatic Environment: A Review. Chemosphere, vol. 251, p. 126351, 2020, https://doi.org/10.1016/j.chemosphere.2020.126351.
10. Stahlmann, R., Kühner, S., Shakibaei, M., Schwabe, R., Flores, J., Evander, S., and Van Sickle, D., Chondrotoxicity of Ciprofloxacin in Immature Beagle Dogs: Immunohistochemistry, Electron Microscopy and Drug Plasma Concentrations. Arch. Toxicol., vol. 73, pp. 564-572, 2000, https://doi.org/10.1007/s002040050009.
11. Azriouil, M., Aghris, S., Matrouf, M., Loudiki, A., Laghrib, F., Farahi, A., Bakasse, M., Saqrane, S., Lahrich, S., and El Mhammedi, M., Efficacy of Clay Materials for Ciprofloxacin Antibiotic Analysis in Urine and Pharmaceutical Products. Mater. Chem. Phys., vol. 279, p. 125787, 2022, https://doi.org/10.1016/j.matchemphys.2022.125787.
12. Wahab, M., Zahoor, M., Muhammad Salman, S., Kamran, A. W., Naz, S., Burlakovs, J., Kallistova, A., Pimenov, N., and Zekker, I., Adsorption-Membrane Hybrid Approach for the Removal of Azithromycin from Water: An Attempt to Minimize Drug Resistance Problem. Water, vol. 13, no. 14, p. 1969, 2021, https://doi.org/10.3390/w13141969.
13. Nasrollahi, N., Vatanpour, V., and Khataee, A., Removal of Antibiotics from Wastewaters by Membrane Technology: Limitations, Successes, and Future Improvements. Sci. Total Environ., vol. 838, p. 156010, 2022, https://doi.org/10.1016/j.scitotenv.2022.156010.
14. Orimolade, B. O., Oladipo, A. O., Idris, A. O., Usisipho, F., Azizi, S., Maaza, M., Lebelo, S. L., and Mamba, B. B., Advancements in Electrochemical Technologies for the Removal of Fluoroquinolone Antibiotics in Wastewater: A Review. Sci. Total Environ., vol. 881, p. 163522, 2023, https://doi.org/10.1016/j.scitotenv.2023.163522.
15. Toyos-Rodríguez, C., Valero-Calvo, D., and de la Escosura-Muñiz, A., Advances in the Screening of Antimicrobial Compounds Using Electrochemical Biosensors: Is There Room for Nanomaterials? Anal. Bioanal. Chem., vol. 415, no. 6, pp. 1107-1121, 2023, https://doi.org/10.1007/s00216-022-04449-x.
16. Wu, D., Karimi-Maleh, H., Liu, X., and Fu, L., Bibliometrics Analysis of Research Progress of Electrochemical Detection of Tetracycline Antibiotics. J. Anal. Methods Chem., vol. 2023, p. 6443610, 2023, https://doi.org/10.1155/2023/6443610.

17. Zheng, S., Wang, Y., Chen, C., Zhou, X., Liu, Y., Yang, J., Geng, Q., Chen, G., Ding, Y., and Yang, F., Current Progress in Natural Degradation and Enhanced Removal Techniques of Antibiotics in the Environment: A Review. Int. J. Environ. Res. Public Health, vol. 19, no. 17, p. 10919, 2022, https://doi.org/10.3390/ijerph191710919.
18. Calcio Gaudino, E., Canova, E., Liu, P., Wu, Z., and Cravotto, G., Degradation of Antibiotics in Wastewater: New Advances in Cavitational Treatments. Molecules, vol. 26, no. 3, p. 617, 2021, https://doi.org/10.3390/molecules26030617.
19. Ahmad, F., Zhu, D., and Sun, J., Environmental Fate of Tetracycline Antibiotics: Degradation Pathway Mechanisms, Challenges, and Perspectives. Environ. Sci. Eur., vol. 33, no. 1, p. 64, 2021, https://doi.org/10.1186/s12302-021-00505-y.
20. Cruz-Cruz, A., Rivas-Sanchez, A., Gallareta-Olivares, G., González-González, R. B., Cárdenas-Alcaide, M. F., Iqbal, H., and Parra-Saldívar, R., Carbon-Based Materials: Adsorptive Removal of Antibiotics from Water. Water Emerg. Contam. & Nanoplastics, vol. 2, no. 1, p. 2, 2023, https://doi.org/10.20517/wecn.2022.19.
21. Javadi, E., Baghdadi, M., Taghavi, L., and Ahmad Panahi, H., Removal of 4-Nonylphenol from Surface Water and Municipal Wastewater Effluent Using Three-Dimensional Graphene Oxide–Chitosan Aerogel Beads. Int. J Environ. Res., vol. 14, pp. 513-526, 2020, https://doi.org/10.1007/s41742-020-00272-3.
22. Chatzimarkou, A. and Stalikas, C., Adsorptive Removal of Estriol from Water Using Graphene-Based Materials and Their Magnetite Composites: Heterogeneous Fenton-Like Non-Toxic Degradation on Magnetite/Graphene Oxide. Int. J Environ. Res., vol. 14, pp. 269-287, 2020, https://doi.org/10.1007/s41742-020-00255-4.
23. Bielawski, C. W., Dreyer, D., Park, S., and Ruoff, R., The Chemistry of Grapheme Oxide. Chem. Soc. Rev, vol. 39, no. 1, pp. 228-240, 2010, https://doi.org/10.1039/B917103G.
24. Lebron, Y. A. R., Moreira, V. R., Drumond, G. P., Gomes, G. C. F., da Silva, M. M., de Oliveira Bernardes, R., Jacob, R. S., Viana, M. M., de Vasconcelos, C. K. B., and de Souza Santos, L. V., Statistical Physics Modeling and Optimization of Norfloxacin Adsorption onto Graphene Oxide. Colloids Surf. A Physicochem. Eng. Asp., vol. 606, p. 125534, 2020, https://doi.org/10.1016/j.colsurfa.2020.125534.
25. Gupta, V. K., Agarwal, S., Asif, M., Fakhri, A., and Sadeghi, N., Application of Response Surface Methodology to Optimize the Adsorption Performance of a Magnetic Graphene Oxide Nanocomposite Adsorbent for Removal of Methadone from the Environment. J. Colloid Interface Sci., vol. 497, pp. 193-200, 2017, https://doi.org/10.1016/j.jcis.2017.03.006.
26. Çalışkan Salihi, E., Wang, J., Kabacaoğlu, G., Kırkulak, S., and Šiller, L., Graphene Oxide as a New Generation Adsorbent for the Removal of Antibiotics from Waters. Sep. Sci. Technol., vol. 56, no. 3, pp. 453-461, 2021, https://doi.org/10.1080/01496395.2020.1717533.
27. Ramesha, G., Kumara, A. V., Muralidhara, H., and Sampath, S., Graphene and Graphene Oxide as Effective Adsorbents toward Anionic and Cationic Dyes. J. Colloid Interface Sci., vol. 361, no. 1, pp. 270-277, 2011, https://doi.org/10.1016/j.jcis.2011.05.050.
28. Boeykens, S. P., Saralegui, A., Caracciolo, N., and Piol, M. N., Agroindustrial Waste for Lead and Chromium Biosorption. J. Sustain. Dev. Energy Water Environ. Syst., vol. 6, no. 2, pp. 341-350, 2018, https://doi.org/10.13044/j.sdewes.d5.0184.
29. Tenev, M. D., Farías, A., Torre, C., Fontana, G., Caracciolo, N., and Boeykens, S. P., Cotton Industry Waste as Adsorbent for Methylene Blue. J. Sustain. Dev. Energy Water Environ. Syst., vol. 7, no. 4, pp. 667-677, 2019, https://doi.org/10.13044/j.sdewes.d7.0269.
30. Mondal, M. K., Mishra, G., and Kumar, P., Adsorption of Cadmium (Ii) and Chromium (Vi) from Aqueous Solution by Waste Marigold Flowers. J. Sustain. Dev. Energy Water Environ. Syst., vol. 3, no. 4, pp. 405-415, 2015, https://doi.org/10.13044/j.sdewes.2015.03.0030.

31. Ndagijimana, P., Liu, X., Xu, Q., Lai, D., Wang, G., Pan, B., and Wang, Y., Cassava Flour Extracts Solution to Induce Gelatin Cross-Linked Activated Carbon-Graphene Oxide Composites: The Adsorption Performance of Dyes from Aqueous Media. Environ. Adv., vol. 5, p. 100079, 2021, https://doi.org/10.1016/j.envadv.2021.100079.
32. Chen, N., Huang, M., Liu, C., Fang, G., Liu, G., Sun, Z., Zhou, D., Gao, J., and Gu, C., Transformation of Tetracyclines Induced by Fe (Iii)-Bearing Smectite Clays under Anoxic Dark Conditions. Water Res., vol. 165, p. 114997, 2019, https://doi.org/10.1016/j.watres.2019.114997.
33. Kyzas, G. Z. and Matis, K. A., Nanoadsorbents for Pollutants Removal: A Review. J. Mol. Liq., vol. 203, pp. 159-168, 2015, https://doi.org/10.1016/j.molliq.2015.01.004.
34. Chen, X. and Ye, N., A Graphene Oxide Surface–Molecularly Imprinted Polymer as a Dispersive Solid-Phase Extraction Adsorbent for the Determination of Cefadroxil in Water Samples. RSC Adv., vol. 7, no. 54, pp. 34077-34085, 2017, https://doi.org/10.1039/C7RA02985C.
35. Upoma, B. P., Yasmin, S., Ali Shaikh, M. A., Jahan, T., Haque, M. A., Moniruzzaman, M., and Kabir, M. H., A Fast Adsorption of Azithromycin on Waste-Product-Derived Graphene Oxide Induced by H-Bonding and Electrostatic Interactions. ACS omega, vol. 7, no. 34, pp. 29655-29665, 2022, https://doi.org/10.1021/acsomega.2c01919.
36. Alishiri, M., Abdollahi, S. A., Neysari, A. N., Ranjbar, S. F., Abdoli, N., and Afsharjahanshahi, M., Removal of Ciprofloxacin and Cephalexin Antibiotics in Water Environment by Magnetic Graphene Oxide Nanocomposites; Optimization Using Response Surface Methodology. Results Eng., vol. 20, p. 101507, 2023, https://doi.org/10.1016/j.rineng.2023.101507.
37. Khiam, G. K., Karri, R. R., Mubarak, N. M., Khalid, M., Walvekar, R., Abdullah, E. C., and Rahman, M. E., Modelling and Optimization for Methylene Blue Adsorption Using Graphene Oxide/Chitosan Composites Via Artificial Neural Network-Particle Swarm Optimization. Mater. Today Chem., vol. 24, p. 100946, 2022, https://doi.org/10.1016/j.mtchem.2022.100946.
38. Khoshraftar, Z., Masoumi, H., and Ghaemi, A., Experimental, Response Surface Methodology (Rsm) and Mass Transfer Modeling of Heavy Metals Elimination Using Dolomite Powder as an Economical Adsorbent. Case Stud. Chem. Environ. Eng., vol. 7, p. 100329, 2023, https://doi.org/10.1016/j.cscee.2023.100329.
39. Xu, Z., Zhou, Y., Sun, Z., Zhang, D., Huang, Y., Gu, S., and Chen, W., Understanding Reactions and Pore-Forming Mechanisms between Waste Cotton Woven and Fecl3 During the Synthesis of Magnetic Activated Carbon. Chemosphere, vol. 241, p. 125120, 2020, https://doi.org/10.1016/j.chemosphere.2019.125120.
40. Akhavan, O., Bijanzad, K., and Mirsepah, A., Synthesis of Graphene from Natural and Industrial Carbonaceous Wastes. RSC Adv., vol. 4, no. 39, pp. 20441-20448, 2014, https://doi.org/10.1039/C4RA01550A.
41. Sujiono, E. H., Zabrian, D., Dahlan, M., Amin, B., and Agus, J., Graphene Oxide Based Coconut Shell Waste: Synthesis by Modified Hummers Method and Characterization. Heliyon, vol. 6, no. 8, p. e04568, 2020, https://doi.org/10.1016/j.heliyon.2020.e04568.
42. Li, F., Zhao, D. L., Bai, L. Z., and Zhang, D. D., Fabrication of Nano Hollow Graphene Oxide Spheres Via Water-in-Oil Emulsion. Appl. Mech. Mater., vol. 320, pp. 540-543, 2013, https://doi.org/10.4028/www.scientific.net/AMM.320.540.
43. Chen, H., Gao, B., and Li, H., Removal of Sulfamethoxazole and Ciprofloxacin from Aqueous Solutions by Graphene Oxide. J. Hazard. Mater., vol. 282, pp. 201-207, 2015, https://doi.org/10.1016/j.jhazmat.2014.03.063.
44. Surekha, G., Krishnaiah, K. V., Ravi, N., and Suvarna, R. P., "Ftir, Raman and Xrd Analysis of Graphene Oxide Films Prepared by Modified Hummers Method," in J. Phys. Conf. Ser., 2020, vol. 1495, no. 1, p. 012012: IOP Publishing..

45. Kanta, U.-a., Thongpool, V., Sangkhun, W., Wongyao, N., and Wootthikanokkhan, J., Preparations, Characterizations, and a Comparative Study on Photovoltaic Performance of Two Different Types of Graphene/Tio 2 Nanocomposites Photoelectrodes. J. Nanomater., vol. 2017, 2017, https://doi.org/10.1155/2017/2758294.
46. Kim, Y. S., Hanif, M. A., Song, H., Kim, S., Cho, Y., Ryu, S.-K., and Kim, H. G., Wood-Derived Graphite: A Sustainable and Cost-Effective Material for the Wide Range of Industrial Applications. Crystals, vol. 14, no. 4, p. 309, 2024, https://doi.org/10.3390/cryst14040309.
47. Hegde, S. S. and Bhat, B. R., Biomass Waste-Derived Porous Graphitic Carbon for High-Performance Supercapacitors. Journal of Energy Storage, vol. 76, p. 109818, 2024, https://doi.org/10.1016/j.est.2023.109818.
48. Tohamy, H.-A. S., Anis, B., Youssef, M. A., Abdallah, A., El-Sakhawy, M., and Kamel, S., Preparation of Eco-Friendly Graphene Oxide from Agricultural Wastes for Water Treatment. Desalin. Water Treat., vol. 191, pp. 250-262, 2020, https://doi.org/10.5004/dwt.2020.25652.
49. Paulchamy, B., Arthi, G., and Lignesh, B., A Simple Approach to Stepwise Synthesis of Graphene Oxide Nanomaterial. J. Nanomed. Nanotechnol., vol. 6, no. 1, p. 1, 2015, https://doi.org/10.4172/2157-7439.1000253.
50. Jiao, X., Qiu, Y., Zhang, L., and Zhang, X., Comparison of the Characteristic Properties of Reduced Graphene Oxides Synthesized from Natural Graphites with Different Graphitization Degrees. RSC Adv., 10.1039/C7RA10809E vol. 7, no. 82, pp. 52337-52344, 2017, https://doi.org/10.1039/C7RA10809E.
51. Özgan, Ş. and Eskalen, H., Electrical Properties of the Octyl Cyanobiphenyl Nematic Liquid Crystal Dispersed with Graphene Oxide. J. Mater. Sci. Mater. Electron., vol. 31, pp. 19787-19796, 2020, https://doi.org/10.1007/s10854-020-04503-3.
52. Cao, N. and Zhang, Y., Study of Reduced Graphene Oxide Preparation by Hummers' Method and Related Characterization. J. Nanomater., vol. 2015, pp. 2-2, 2015, https://doi.org/10.1155/2015/168125.
53. Somanathan, T., Prasad, K., Ostrikov, K., Saravanan, A., and Mohana Krishna, V., Graphene Oxide Synthesis from Agro Waste. Nanomaterials, vol. 5, no. 2, pp. 826-834, 2015, https://doi.org/10.3390/nano5020826.
54. Salari, M., Optimization by Box–Behnken Design and Synthesis of Magnetite Nanoparticles for Removal of the Antibiotic from an Aqueous Phase. Adsorp. Sci. Technol., vol. 2022, 2022, https://doi.org/10.1155/2022/1267460.
55. Redhwan, A., Azmi, W., Sharif, M., Zawawi, N., and Ariffin, S. Z., "Utilization of Response Surface Method (Rsm) in Optimizing Automotive Air Conditioning (Aac) Performance Exerting Al2o3/Pag Nanolubricant," in J. Phys. Conf. Ser., 2020, vol. 1532, no. 1, p. 012003: IOP Publishing, https://doi.org/10.1088/1742-6596/1532/1/012003..
56. Irfan, M., Waqas, S., Arshad, U., Khan, J. A., Legutko, S., Kruszelnicka, I., Ginter-Kramarczyk, D., Rahman, S., and Skrzypczak, A., Response Surface Methodology and Artificial Neural Network Modelling of Membrane Rotating Biological Contactors for Wastewater Treatment. Materials, vol. 15, no. 5, p. 1932, 2022, https://doi.org/10.3390/ma15051932.
57. Konkena, B. and Vasudevan, S., Understanding Aqueous Dispersibility of Graphene Oxide and Reduced Graphene Oxide through Pka Measurements. J Phys. Chem. Lett., vol. 3, no. 7, pp. 867-872, 2012, https://doi.org/10.1021/jz300236w.
58. Peng, B., Chen, L., Que, C., Yang, K., Deng, F., Deng, X., Shi, G., Xu, G., and Wu, M., Adsorption of Antibiotics on Graphene and Biochar in Aqueous Solutions Induced by Π-Π Interactions. Sci. Rep., vol. 6, no. 1, p. 31920, 2016, https://doi.org/10.1038/srep31920.
59. Rostamian, R. and Behnejad, H., A Comprehensive Adsorption Study and Modeling of Antibiotics as a Pharmaceutical Waste by Graphene Oxide Nanosheets. Ecotoxicol. Environ. Saf., vol. 147, pp. 117-123, 2018, https://doi.org/10.1016/j.ecoenv.2017.08.019.

60. Ghadiri, S. K., Alidadi, H., Tavakkoli Nezhad, N., Javid, A., Roudbari, A., Talebi, S. S., Mohammadi, A. A., Shams, M., and Rezania, S., Valorization of Biomass into Amine-Functionalized Bio Graphene for Efficient Ciprofloxacin Adsorption in Water-Modeling and Optimization Study. Plos one, vol. 15, no. 4, p. e0231045, 2020, https://doi.org/10.1371/journal.pone.0231045.
61. Igwegbe, C. A., Oba, S. N., Aniagor, C. O., Adeniyi, A. G., and Ighalo, J. O., Adsorption of Ciprofloxacin from Water: A Comprehensive Review. J. Ind. Eng. Chem., vol. 93, pp. 57-77, 2021, https://doi.org/10.1016/j.jiec.2020.09.023.
62. Wakejo, W. K., Meshasha, B. T., Kang, J. W., and Chebude, Y., Enhanced Ciprofloxacin Removal from Aqueous Solution Using a Chemically Modified Biochar Derived from Bamboo Sawdust: Adsorption Process Optimization with Response Surface Methodology. Adsorp. Sci. Technol., vol. 2022, pp. 1-23, 2022, https://doi.org/10.1155/2022/2699530.

Paper submitted: 26.12.2023
Paper revised: 02.06.2024
Paper accepted: 03.06.2024